Microphysical Structures of Early-Winter Snow Clouds during a Cold Air Outbreak of December 23−25, 2010

Ryoichi Watanabe[1], Kenji Suzuki[2], Tetsuya Kawano[3], and Soichiro Sugimoto[4]
[1]*Graduate School of Agriculture, Yamaguchi University, Yamaguchi, Japan*
[2]*Department of Biological and Environmental Sciences, Yamaguchi University, Yamaguchi, Japan*
[3]*Department of Earth and Planetary Sciences, Kyushu University, Fukuoka, Japan*
[4]*Civil Engineering Research Laboratory, Central Research Institute of Electric Power Industry, Abiko, Japan*

Abstract

A series of videosondes that were continuously launched revealed the microphysical structures of snow clouds during the entire period of an intense cold air outbreak that occurred during December 23−25, 2010. The evolution of the microphysical features of graupel and snowflakes associated with the cold air outbreak were examined. It was found that the precipitation particle distributions in the snow clouds varied as the development of the cold air outbreak progressed. Graupel was the predominant precipitation particle throughout the cold air outbreak, while the number of snowflakes was increasing in the latter half of the period. When the lightning activity was relatively weak, high concentrations of graupel were located at lower level warmer than −10°C. It is suggested that lightning activity is associated with the vertical distribution of graupel.

(**Citation:** Watanabe, R., K. Suzuki, T. Kawano, and S. Sugimoto, 2014: Microphysical structures of early-winter snow clouds during a cold air outbreak of December 23−25, 2010. *SOLA*, **10**, 62−66, doi:10.2151/sola.2014-012.)

1. Introduction

During Siberian cold air outbreaks in winter, the relatively warm sea supplies a large amount of heat and moisture into the atmosphere, and numerous convective clouds then form and develop over the Sea of Japan. These clouds often bring heavy snowfall over the coastal areas of Hokuriku, which is the northwestern region of Honshu that faces the Sea of Japan, and this heavy snowfall sometimes causes problems, such as snow accretion and snowbound traffic. To prevent these problems caused by snow, it is important to understand the mechanism of snowfall and to predict the temporal and spatial patterns of snowfall. In order to understand the mechanism of snowfall, it is essential to investigate the microphysical structures of clouds, such as the types, sizes, and concentrations of precipitation particles. In the Hokuriku coastal regions, intense lightning activity is often observed during early winter snowfall, and such an event is popularly referred to as "yuki-okoshi" in Japanese, which means the event is an indication of the beginning of winter. Investigations of the microphysical structures of snow clouds are also important to understand the mechanism of winter lightning (e.g., Takahashi 1978; Takahashi et al. 1999).

Many microphysical and observational studies of winter snow clouds have been made. Mizuno (1992) reported that graupel precipitation is predominant in winter over the coastal regions of Hokuriku by conducting a statistical analysis using routine surface observation data. Harimaya and Kanemura (1995) clarified that the riming process is predominant and plays a more important role in the growth of snow particles in the coastal regions compared to the inland regions of the Ishikari Plain of Hokkaido by using a Doppler radar and surface observations. They also showed that the riming process is predominant and associated with strong updrafts in the developing and mature stages of snow clouds.

Ohigashi and Tsuboki (2005) observed the kinematical and microphysical structures of double snowbands that remained along the coastal region of Hokuriku using Doppler and dual-polarization radars. They found that graupel was dominant in the snowband with a strong updraft, while snowflakes were dominant in the snowband with a weak updraft. However, their understanding of the detailed microphysical structures of the clouds was limited, since the cloud microphysics was estimated by using polarimetric parameters.

In-situ observations are essential to gain a better understanding of the detailed microphysical structures of a cloud. Many observations within snow clouds via balloon-borne sondes have been conducted (e.g., Magono and Lee 1973; Matsuo et al. 1994; Murakami et al. 1994, 2003; Kusunoki et al. 2004, 2005).

Videosondes (Takahashi 1990) are powerful tools for observing solid precipitation particles such as graupel and snowflakes, since they can measure precipitation particles without contact and can obtain images of the particles as they fall through the air. They also have an advantage over the film-capture-type sondes (Magono and Tazawa 1966). Takahashi et al. (1999) conducted videosonde observations of winter monsoon snow clouds in Hokuriku. They classified their videosonde soundings into different stages of cloud life on the basis of the updraft in the clouds, and discussed the electrical structures at each stage. In the previous studies, videosondes were not launched continually at short intervals because of the cost and technical constraints. Consequently, the microphysical structures of clouds were discussed using composited videosonde data (e.g., Suzuki et al. 2013). Therefore, the evolution of the microphysical structures of the snow clouds associated with cold air outbreaks is unclear.

In order to understand the process of heavy snowfall and the electric charge distribution in Hokuriku during a winter thunderstorm, an observation campaign using videosondes was conducted in Kashiwazaki (37.35°N, 138.58°E), which is located in the Hokuriku area of Japan, in the early winter of 2010 (Sugimoto et al. 2011). A total of 15 videosondes were launched into snow clouds that were associated with the cold air outbreak that occurred from December 23 through December 25. We succeeded in continuously launching the videosondes, and the vertical distributions of the precipitation particles in the snow clouds that developed through the entire stage of the cold air outbreak are revealed. To the best of our knowledge, this was the first time that numerous videosondes were launched into snow clouds continually and frequently during a cold air outbreak. In this paper, the evolution of the microphysical structures associated with the cold air outbreak in early winter is investigated.

2. Videosonde

Balloon-borne videosondes can obtain images of precipitation particles and measure their vertical distribution in a cloud. The videosonde that was reduced in size and weight by Suzuki et al. (2012) was used in the present study. The videosondes consist of a CCD camera, a strobe, an infrared sensor, and a transmitter.

Corresponding author: Kenji Suzuki, Department of Biological and Environmental Sciences, Yamaguchi University, 1677-1 Yoshida, Yamaguchi 753-8515, Japan. E-mail: kenjis@yamaguchi-u.ac.jp.

When particles interrupt the infrared beam the strobe is triggered, and particle images are then captured by the CCD camera. Particle images are transmitted to the receiving system at the surface by a 1680-MHz carrier wave and recorded on videotapes. The recorded precipitation particles are classified as raindrops, frozen drops, graupel, ice crystals, or snowflakes on the basis of their transparency and shape, as described by Takahashi and Keenan (2004). Vertical profiles of atmospheric pressure, temperature, humidity, and wind are obtained from a Vaisala RS-92 radiosonde that is attached to each videosonde.

3. Results and discussion

3.1 Weather conditions

On December 23, 2010, a depression developed and passed slowly along the northern areas of Japan. After the passing of the depression, the winter monsoon was enhanced, and snow cloud streets then developed over the Sea of Japan.

Figure 1 shows the surface temperatures and surface winds at the Kashiwazaki Automated Meteorological Data Acquisition System (AMeDAS) station, and the number of cloud-to-ground (C-G) lightning strikes that were observed in a 2° square area in latitude and longitude, with Kashiwazaki at its center, from December 23 to 25, 2010. C-G lightning strikes were observed by the Japan Lightning Detection Network (JLDN; e.g., Ishii et al. 2006).

As the cold air outbreak developed, the surface temperature decreased from 10.5°C (1200 Japan Standard Time: JST, December 23) to 2.5°C (1200 JST, December 24). On December 25, the surface temperature was below 3°C the entire day, and then increased to 6.1°C at 1200 JST on December 26. During the cold air outbreak, a northwesterly wind was primarily observed at the surface on December 24. The wind direction changed to westerly and the wind speed increased on December 25. C-G lightning was actively observed up until the morning of December 24. There was no C-G lightning from 1200−2300 JST on December 24. A small number of C-G lightning strikes were observed on December 25.

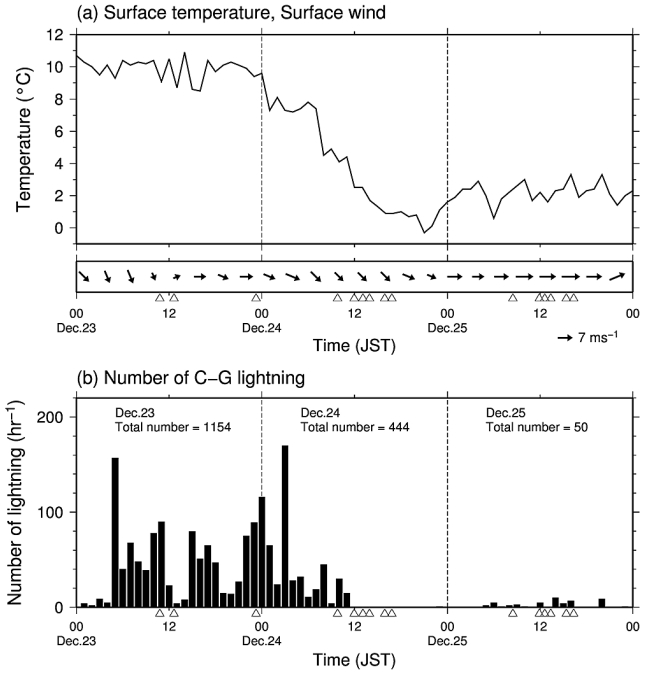

Fig. 1. Time series of (a) the surface temperature and surface wind at Kashiwazaki and (b) the number of C-G lightning strikes observed in a 2° square area in latitude and longitude, with Kashiwazaki at its center, from December 23 to 25, 2010. The C-G lightning data domain (36.35°N−38.35°N, 137.58°E−139.58°E) corresponds to the area in described in Fig. 2. Triangle marks show the launches of videosondes.

Figure 2 shows precipitation intensity derived from the Japan Meteorological Agency (JMA) radars in each case of 15 videosonde launchings. On December 23, the row of precipitation area which extended to the east-southeast from west-northwest was dominant. After the early morning of December 24, the radar echoes extended parallel to the coastal region near the observation site. The surface weather charts for December 24 and 25 show a typical Japanese winter monsoon pattern (not shown).

3.2 Classification of the stages of the cold air outbreak

The videosonde soundings were classified into three stages for the cold air outbreak, depending on the evolution of the surface temperature. The cold air outbreak stage (referred to as the CAO stage) is defined as the period from 0100 JST, which was when the surface temperature decreased by more than 2°C in comparison to the average temperature of the previous 6 hours, to 2100 JST, which was when the lowest surface temperature was recorded, on December 24. The Pre-CAO and Post-CAO stages are defined as the periods before and after the CAO stage, respectively.

A total of 15 videosondes were launched into the snow clouds that were associated with the cold air outbreak, as described in Table 1. During the Pre-CAO stage (videosondes #1, #2, and #3), the videosondes were launched when the rain was observed at the surface observation site, and then it changed to sleet in the morning of December 24. During the CAO stage (videosondes #4, #5, #6, #7, #8, and #9), the main precipitation particle observed at the surface prior to the launch of videosonde #5 was graupel. The majority of the particles at the surface then changed to snowflakes. During the Post-CAO stage (videosondes #10, #11, #12, #13, #14, and #15), the main precipitation particle observed at the surface was either graupel or snowflakes.

Images of raindrops and frozen drops were transmitted from the videosondes #1−4 below 0.5 km in altitude (Fig. 3a, b). Graupel was observed throughout the clouds. A few snowflakes were observed at the upper levels (above 3 km) of the clouds. After videosonde #5 was launched, the other videosondes did not transmit any images of raindrops or frozen drops (Fig. 3c, d). Numerous snowflakes were observed in clouds as well as graupel after the case of videosonde #6. As shown in Table 1, the height of the cloud tops during the CAO stage were relatively low; cloud top is defined as the maximum height at which the precipitation particles were observed by the videosonde. The updrafts in the clouds were estimated as the differences between the 10-second averages of the sonde ascent rate and the ascent rate averaged from the surface to cloud top, in accordance with Asai (1968). During the CAO stage, the updrafts were relatively weak.

3.3 Microphysical features

Here we focus on the microphysical features of graupel and snowflakes at each stage. Table 2 shows the microphysical features during each stage. The number density and mass density were calculated for every 500-m layer from the surface. The number density was estimated from the particles larger than 0.5 mm in diameter since the minimum performance of the infrared sensor in the videosonde is to respond completely to a particle that is 0.5 mm or larger in diameter (Suzuki et al. 2012, 2013). The mass of the particles was estimated from the diameters obtained from the videosonde observations by assuming that the particles are spherical in shape. It is known that the density of an ice particle depends on its formation process. For example, Pruppacher and Klett (1997) reported that the density of graupel varies from 0.1 to 0.85 g cm^{-3}. In the present study, however, the density of graupel and snowflakes were assumed to be 0.3 g cm^{-3} and 0.1 g cm^{-3}, respectively, which are often used in cloud models.

As shown in Table 2, the mean diameters of graupel in the Pre-CAO stage were larger than in the CAO and Post-CAO stages. The maximum diameter and maximum number density of graupel that averaged on each stage showed maximum values in the CAO stage. The maximum mass density decreased as the cold air outbreak developed.

The maximum diameter and maximum mass density of a snowflake increased in the CAO and Post-CAO stages. The max-

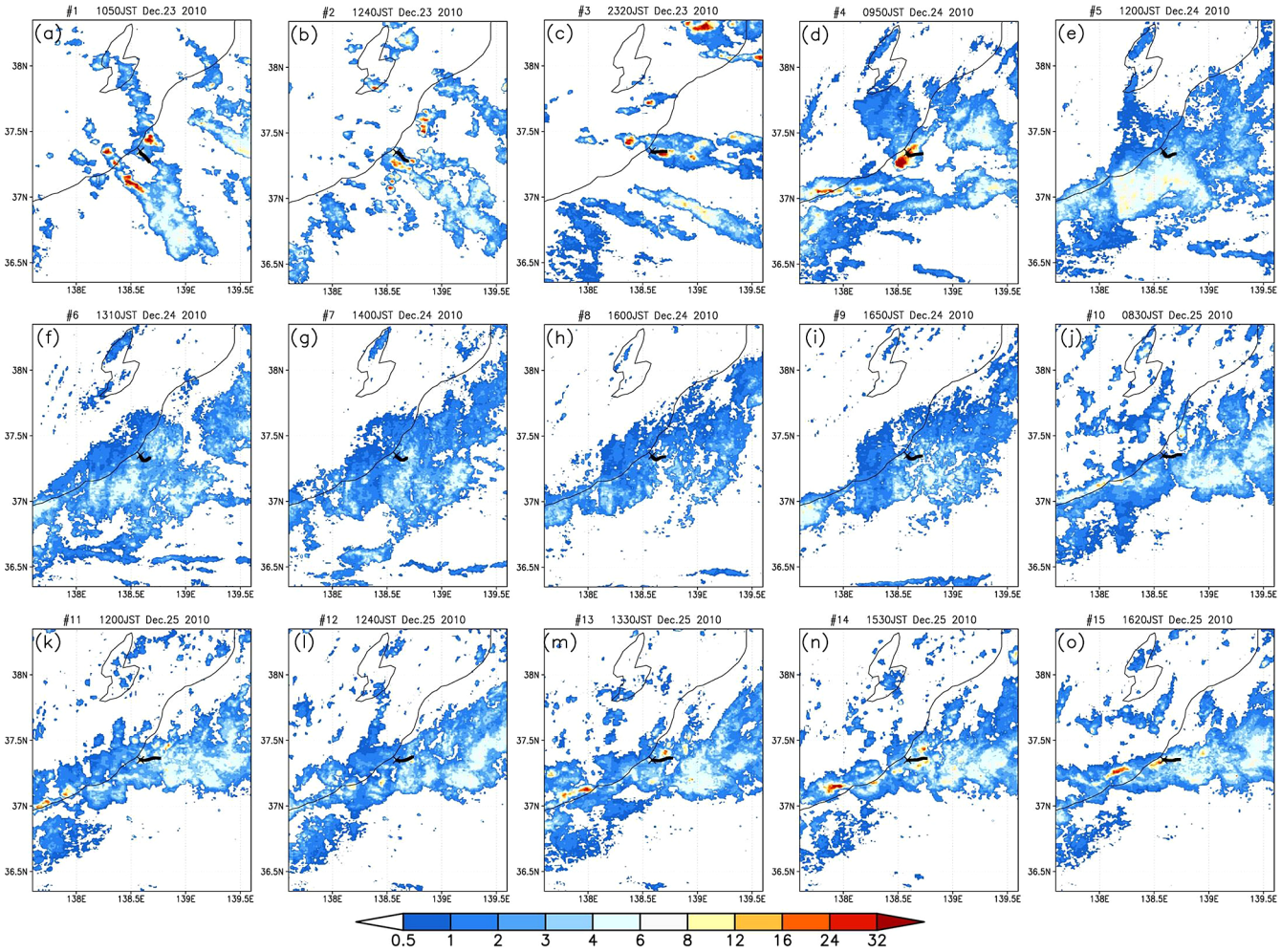

Fig. 2. Precipitation intensity (mm h^{-1}) derived from the JMA radars of (a) 1050 JST, December 23, (b) 1240 JST, December 23, (c) 2320 JST, December 23, (d) 0950 JST, December 24, (e) 1200 JST, December 24, (f) 1310 JST, December 24, (g) 1400 JST, December 24, (h) 1600 JST, December 24, (i) 1650 JST, December 24, (j) 0830 JST, December 25, (k) 1200 JST, December 25, (l) 1240 JST, December 25, (m) 1330 JST, December 25, (n) 1530 JST, December 25, (o) 1620 JST, December 25. The location of the videosonde launching site is shown as X mark. Black dots indicate the trajectories of the videosondes (a) #1, (b) #2, (c) #3, (d) #4, (e) #5, (f) #6, (g) #7, (h) #8, (i) #9, (j) #10, (k) #11, (l) #12, (m) #13, (n) #14, (o) #15 every minute for 15 minutes after launching.

Table 1. Details of the launching of the videosondes.

Sonde No.	Launch		Surface Temp (°C)	Cloud Top*		Maximum Updraft (m s^{-1})	Classification
	Date	Time (JST)		Height (km)	Temp (°C)		
1	Dec.23	10:47	8.5	3.8	−16.7	2.1	Pre-CAO
2	Dec.23	12:38	8.9	4.7	−25.2	3.7	
3	Dec.23	23:14	6.8	4.1	−21.8	3.2	
4	Dec.24	09:47	4.4	4.8	−31.4	4.7	CAO
5	Dec.24	11:56	2.8	3.3	−20.6	3.7	
6	Dec.24	13:05	2.0	2.9	−18.3	1.9	
7	Dec.24	13:55	0.9	2.7	−17.5	1.6	
8	Dec.24	15:53	0.8	2.6	−18.3	2.4	
9	Dec.24	16:49	0.7	2.7	−19.3	2.4	
10	Dec.25	08:28	1.9	3.7	−26.3	3.8	Post-CAO
11	Dec.25	11:54	1.3	4.2	−30.3	5.7	
12	Dec.25	12:36	1.2	3.6	−25.1	1.8	
13	Dec.25	13:24	1.7	4.1	−29.1	3.9	
14	Dec.25	15:23	1.7	3.8	−26.0	2.8	
15	Dec.25	16:20	1.7	3.8	−25.3	6.3	

*The maximum height at which the precipitation particles were observed by videosonde

imum number densities of snowflakes in the CAO and Post-CAO stages were larger than those in the Pre-CAO stage. The mean diameter of the snowflakes differed very little among the stages.

The mass contribution ratio is a parameter that indicates the contribution of each precipitation particle to the total precipitation. The mass contribution ratio was calculated as the proportion of mass of each particle to the total mass of the precipitation particles obtained throughout the cloud. During the Pre-CAO stage, the mass contribution ratio of graupel was 94.6%. While, during the CAO and Post-CAO stages, it decreased to 87.9% and 84.9%, but that of snowflakes increased to 6.1% and 9.2%, respectively.

3.4 Evolution of the vertical distribution of graupel

The vertical profiles of the number density of graupel varied among each stage. Figure 4 shows vertical distributions of the number density of graupel for every 500-m layer from each videosonde soundings. The dashed lines in the plots indicate the −10°C level that was obtained by the radiosondes. In the Pre-CAO stage, the peak for the number density of graupel is located around an altitude of 2.8 km, at which the temperature was approximately −10°C. The altitude of the maximum number density of graupel shifted to the lower levels as the cold air outbreak developed. During the CAO stage, it was between 0.5 km and 2 km in altitude (between −2.7°C and −12.7°C in temperature) for videosonde #7, which was launched at 1355 JST. During the Post-CAO stage,

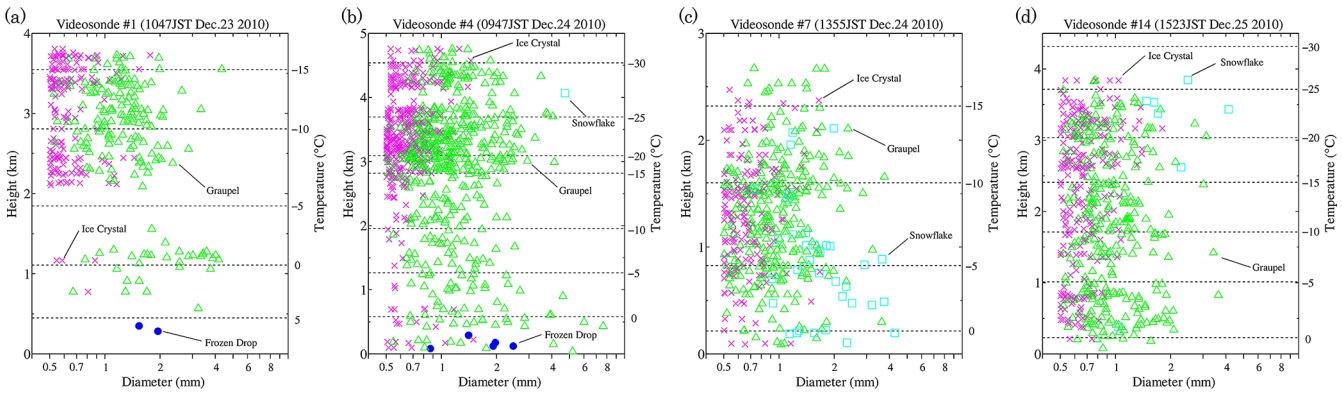

Fig. 3. Size-height diagrams of the precipitation particles observed by videosondes (a) #1 launched at 1047 JST on December 23, (b) #4 at 0947 JST on December 24, (c) #7 at 1355 JST on December 24 and (d) #14 at 1523 JST on December 25. Open circles, solid circles, triangles, crosses and squares indicate raindrops, frozen drops, graupel, ice crystals and snowflakes, respectively.

Table 2. Microphysical features of graupel and snowflakes obtained from videosonde soundings during the cold air outbreak.

Sonde No.	Classification	Mean Diameter (mm)		Max Diameter (mm)		Max Number Density (m^{-3})		Max Mass Density (mg m^{-3})		Mass Contribution Ratio (%)	
		Graupel	Snowflake	Graupel	Snowflake	Graupel	Snowflake	Graupel	Snowflake	Graupel	Snowflake
1	Pre-CAO	1.46	–	4.35	–	260.0	–	446.5	–	95.2	–
2		1.20	1.60	2.98	1.60	209.1	3.2	112.3	0.7	88.7	0.2
3		1.57	2.85	4.74	3.05	117.7	3.4	278.6	5.1	96.9	1.1
4	CAO	1.30	4.74	7.64	4.74	627.9	3.5	467.9	19.8	93.8	1.2
5		1.25	1.34	4.58	1.88	304.2	16.9	172.9	3.1	94.5	0.6
6		1.27	1.97	4.34	4.21	252.7	53.0	163.8	24.7	76.1	16.7
7		1.07	1.82	3.76	4.30	325.3	41.7	142.4	37.1	79.8	16.2
8		1.10	3.94	3.43	4.69	221.9	10.1	80.9	34.2	72.5	12.3
9		1.17	1.52	3.34	3.28	209.2	45.6	78.4	11.7	87.9	6.2
10	Post-CAO	1.18	2.72	3.41	3.44	167.3	3.9	91.5	8.3	91.4	2.8
11		1.25	–	5.40	–	356.3	–	230.1	–	98.9	–
12		1.23	2.24	2.23	4.48	82.9	25.3	30.9	39.3	35.7	40.6
13		1.41	1.99	4.92	4.27	106.6	27.9	289.8	24.4	78.8	15.1
14		1.02	2.11	3.64	4.16	229.7	9.4	93.0	14.1	88.5	6.0
15		1.27	1.82	3.79	5.09	278.1	34.8	117.2	33.1	83.5	11.5

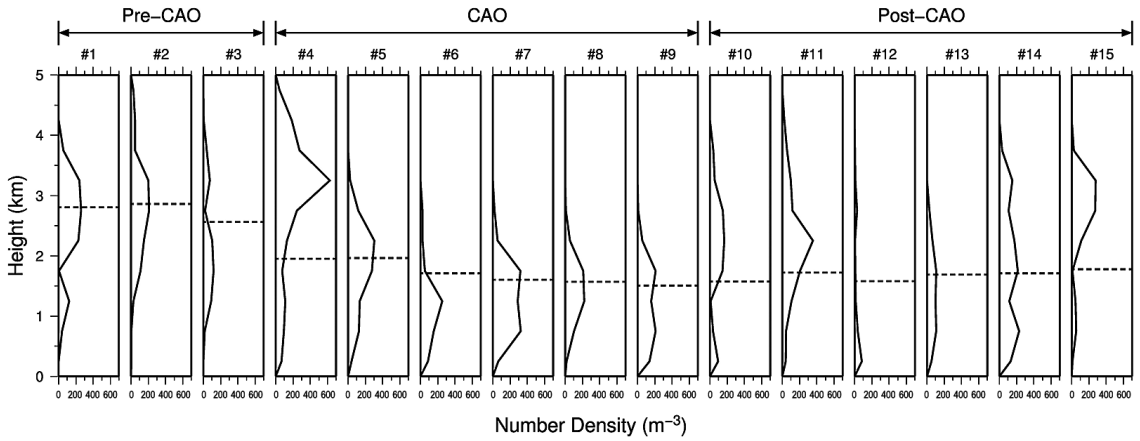

Fig. 4. Vertical distributions of the number density of graupel for every 500-m layer from each videosonde soundings. Dashed lines indicate the locations of the −10°C levels that were obtained from the radiosondes.

the altitude of the maximum number density increased to above 1.7 km (approximately −10°C).

During the CAO stage, two different vertical distributions of graupel were observed. The peaks for the number densities of graupel obtained from videosondes #6, #7, #8, and #9 are located below 1.5 km (−10°C), and their structures differ from those obtained by videosondes #4 and #5. For videosondes #6, #7, #8, and #9, the maximum diameter and maximum number density of graupel were smaller than the other two cases, their cloud tops were lower than 3 km, and the updrafts in the clouds were relatively weak (Table 1).

During this cold air outbreak, as shown in Fig. 1b, C-G light-

ning was active around the observation site until the morning of December 24. Conversely, no C-G lightning was observed from 1200 JST to 2300 JST on December 24. Videosondes #6, #7, #8, and #9 were launched continually during this period, in which there was no C-G lightning. During the Post-CAO stage, when the altitude of the peak number density of graupel increased, C-G lightning was observed. Takahashi (1978) suggested that a large number density of graupel and a change in the charge of graupel at approximately −10°C are critical for the occurrence of lightning. Takahashi et al. (1999) also reported that the charge distributions in clouds varied among the different developing stages of the clouds. These indicate that the weak updrafts and high graupel concentrations at lower levels (warmer than −10°C) are related to the non-occurrence of C-G lightning during the afternoon of December 24. However, the charge distributions in the clouds were not measured in the present study. In order to discuss the relationships between lightning activity and cloud microphysics, such as the vertical distributions of graupel, further videosonde observations that provide both the vertical distributions of the precipitation particles and the electric charges in the clouds will need to be conducted.

4. Summary and conclusions

During an intense cold air outbreak event that occurred from December 23 to 25, 2010, 15 videosondes were successfully launched into snow clouds, and the precipitation particle distributions of the snow clouds were revealed for the entire cold air outbreak. To our knowledge, this was the first time that numerous videosondes were launched into snow clouds continuously within the period of a cold air outbreak.

The 15 videosonde soundings were classified into three stages of the cold air outbreak (the Pre-CAO, CAO, and Post-CAO stages) on the basis of the evolution of the surface temperatures. We found that the precipitation particle distributions and the microphysical features in the clouds were different among the three stages. Graupel mainly contributed to the total precipitation during the Pre-CAO stage. As the graupel mass contribution ratio decreased, the contribution of snowflakes to the total precipitation increased as the cold air outbreak developed.

The vertical distributions of the number densities of graupel varied among the different stages of the cold air outbreak. The altitude of the peak for the number density of graupel was located at lower levels during the late CAO stage, at which the temperature was warmer than −10°C. These results suggest that the evolution of the microphysical structures associated with the cold air outbreak, especially the graupel vertical distributions, is related to the lightning activity.

The evolution of the microphysical structures of the snow clouds were also revealed for all of the stages of the cold air outbreak. The results provide important information for a better understanding of the mechanisms of snowfall and lightning. However, it should be noted that the precipitation particle distributions obtained from videosondes correspond to given trajectories of the videosondes. So, there must be discussion about the spatial representativeness of videosonde data. To show it, the Range Height Indicator (RHI) operation targeting the videosonde in the cloud is one of the effective methods (Suzuki et al. 2013). Unfortunately, in this study, we cloud not conduct the RHI observations during the observation period. In addition, we did not measure the charge distribution in the clouds in the present study. Simultaneous measurements of precipitation particles and their electric charges are needed to determine the relationship between the cloud microphysical structures and lightning activity.

Acknowledgements

We would like to thank Dr. Tsutomu Takahashi for the productive discussions and for his suggestion. We would also like to thank Dr. Mitsuharu Nomura of Central Research Institute of Electric Power Industry and the students of Yamaguchi University and Kyushu University who helped to conduct the videosonde observations in Kashiwazaki for their assistance.

References

Asai, T., 1968: An analysis of convective activity in the atmosphere using rawinsonde data. *Tenki*, **15**, 109−115 (in Japanese).

Harimaya, T., and N. Kanemura, 1995: Comparison of Riming growth of snow particles between coastal and inland areas. *J. Meteor. Soc. Japan*, **73**, 25−36.

Ishii, M., M. Saito, F. Fujii, A. Sugita, and N. Itamoto, 2006: Investigation on LEMP observed by JLDN. 19th International Lightning Detection Conference, No.21, Tucson, Arizona, U.S.A.

Kusunoki, K., M. Murakami, M. Hoshimoto, N. Orikasa, Y. Yamada, H. Mizuno, K. Hamazu, and H. Watanabe, 2004: The characteristics and evolution of orographic snow clouds under weak cold advection. *Mon. Wea. Rev.*, **132**, 174−191.

Kusunoki, K., M. Murakami, N. Orikasa, M. Hoshimoto, Y. Tanaka, Y. Yamada, H. Mizuno, K. Hamazu, and H. Watanabe, 2005: Observations of quasi-stationary and shallow orographic snow clouds: Spatial distributions of supercooled liquid water and snow particles. *Mon. Wea. Rev.*, **133**, 743−751.

Magono, C., and S. Tazawa, 1966: Design of a "snow crystal sonde." *J. Atmos. Sci.*, **23**, 618−625.

Magono, C., and C. W. Lee, 1973: The vertical structure of snow clouds, as revealed by "snow crystal sondes", part 2. *J. Meteor. Soc. Japan*, **51**, 176−190.

Matsuo, T., H. Mizuno, M. Murakami, and Y. Yoshida, 1994: Requisites of graupel formation in snow clouds over the Sea of Japan. *Atmos. Res.*, **32**, 55−74.

Mizuno, H., 1992: Statistical characteristics of graupel precipitation over the Japan Islands. *J. Meteor. Soc. Japan*, **70**, 115−121.

Murakami, M., T. Matsuo, H. Mizuno, and Y. Yamada, 1994: Mesoscale and microscale structures of snow clouds over the Sea of Japan. Part 1: Evolution of microphysical structures in short-lived convective snow clouds. *J. Meteor. Soc. Japan*, **72**, 671−694.

Murakami, M., Y. Yamada, T. Matsuo, K. Iwanami, J. D. Marwitz, and G. Gordon, 2003: The precipitation process in convective cells embedded in deep snow bands over the Sea of Japan. *J. Meteor. Soc. Japan*, **81**, 515−531.

Ohigashi, T., and K. Tsuboki, 2005: Structure and maintenance process of stationary double snowbands along the coastal region. *J. Meteor. Soc. Japan*, **83**, 331−349.

Pruppacher, H. R., and Klett, J. D., 1997: *Microphysics of Clouds and Precipitation.2d ed*. Kluwer Academic Publishers, 954 pp.

Sugimoto, S., K. Suzuki, H. Hirakuchi, M. Nomura, and K. Wada, 2011: Observation using a videosonde for understanding severe storm meteorology −A use of observed data for finding problem in cloud microphysics models−. *Civil Engineering Research Laboratory Rep*. No.N10042.

Suzuki, K., K. Shimizu, T. Ohigashi, K. Tsuboki, S. Oishi, S. Kawamura, K. Nakagawa, K. Yamaguchi, and E. Nakakita, 2012: Development of a new videosonde observation system for in-situ precipitation particle measurements. *SOLA*, **8**, 1−4, doi:10.2151/sola.2012-001.

Suzuki, K., M. Matsuo, E. Nakano, S. Shigeto, K. Yamaguchi, and E. Nakakita, 2014: Graupel in the different developing stages of Baiu monsoon clouds observed by videosondes. *Atmos. Res*., **142**, 100−110, doi:10.1016/j.atmosres.2013.09.020.

Takahashi, T., 1978: Riming electrification as a charge of cloud droplets, drizzle and raindrops. *J. Atmos. Sci.*, **35**, 1536−1548.

Takahashi, 1990: Near absence of lightning in tropical rainfall producing Micronesian thunderstorms. *Geophys. Res. Lett.*, **17**, 2381−2384.

Takahashi, T., and T. D. Keenan, 2004: Hydrometeor mass, number, and space charge distribution in a "Hector" squall line. *J. Geophys. Res.*, **109**, D16208, doi:10.1029/2004JD004667.

Takahashi, T., T. Tajiri, and Y. Sonoi, 1999: Charges on graupel and snow crystals and the electrical structure of winter thunderstorms. *J. Atmos. Sci.*, **56**, 1561−1578.

Manuscript received 16 November 2013, accepted 26 March 2014
SOLA: https://www.jstage.jst.go.jp/browse/sola/